Article

Dynamic Model Used for Describing the Coupled Vibration of Gear Pair and Bearing in the Gearbox

Yan Shuping [1], Dai Peng [2], Shu Da [1], Wang Jianbin [1], Sun Jie [3], Zhang Dabin [3,*] and Hongwei Li [4]

[1] School of Mechanical Engineering, Anhui Polytechnic University, Wuhu, Anhui 241000 China; ysp620@163.com (Y.S.); sd@ahpu.edu.cn (S.D.); wjb@ahpu.edu.cn (W.J.)
[2] State Key Laboratory of Engines, Tianjin University, Tianjin 300072 China; daipeng_ahpu@163.com
[3] School of Mechanical Engineering, Guizhou University, Guiyang, Guizhou 550025 China; 1018451579@qq.com (S.J.)
[4] Anhui Peiji Intelligent Technology Co., LTD, Wuhu, Anhui 241000 China; 4645926@qq.com
* Correspondence: dbzhang@gzu.edu.cn

Abstract: The fault diagnosis of the gearbox is primarily based on the analysis of the harmonic response. However, the generation mechanism of the harmonic response of the gear pair is still not distinctly explained in a healthy gearbox. Therefore, this paper is dedicated to establishing a dynamic model of the gearbox for this issue. In this model, the contact force of the bearing and the meshing stiffness of the gear pair are determined by the Hertz theory and the potential energy method, then the shaft motion is used as the connection to establish the coupling relationship between the gear pair and the bearing. After this dynamic model is confirmed by experiments and existing models, the coupling relationship inside the gearbox and the harmonic response of the gear pair are studied using this model. The result demonstrates that a closed control loop is formed due to the vibration transmission between the gear pair, the bearing and the shaft, and there is a strong coupled vibration between the gear pair and the bearing in the gearbox. Due to the generation of the center distance error, misalignment angle and disorganized meshing process of the gear pair, the meshing stiffness is altered, which excites the harmonic response of the gear pair. When the speed of the gearbox is increased, although the vibration amplitude of the gearbox is increased, the system predominantly vibrates at the fundamental frequency, and the harmonic of the gear pair is also shifted to the low frequency band.

Keywords: gearbox; dynamic model; harmonic response; input speed; coupled vibration

1. Introduction

The gearbox with the gear-shaft-bearing system as the main component is an important transmission mechanism, which is frequently used to transmit mechanical power and control the rotation direction, and is commonly used in wind turbines and various transportation vehicles [1,2]. In order to prevent transmission failure and possible economic losses, during the working process of the gearbox, it is indispensable to distinguish its operating state for removing mechanical faults and replacing new parts, then the safe and reliable operation of the equipment can be accomplished [3,4]. The state detection of the rotating machinery is based on the vibration response analysis, which requires a clear understanding of the vibration mechanism to help evaluate the health status accurately [5,6]. Furthermore, the gearbox is composed of multiple parts, the cooperative operation between the gear pair and the bearing makes the system exhibit a strong vibration transmission and coupling relationship, which makes the vibration mechanism and response of the gearbox extremely complicated, and brings great difficulty to the identification of the operating state [7,8]. Subsequently, it is imperative to establish the dynamic model to study the vibration mechanism and vibration response of the gearbox in depth, and to investigate the coupling relationship between the gear pair and the bearing in the gearbox.

In the research field of fault diagnosis for the gear pair, the mathematical model for describing the vibration response have been proposed and updated successively, another main approach is using a finite element/contact mechanics model to analyze load distribution and contact states [9,10]. The 6 DOFs dynamic model of the gear pair with crack defects was established by Ma [11,12], and the meshing stiffness was calculated under different crack propagation paths, then then the vibration characteristics of the gear pair were summarized. The dynamic model and research method have important reference value for the follow-up research of the gear pair fault diagnosis. Later, a new dynamic model of the cylindrical gear pair with localized spalling defects was proposed by Yu [13], in which the effect of the failure was divided into meshing stiffness reduction and displacement excitation according to the degree of spalling defect, and a correction factor was introduced to explain the influence of the nonlinear elliptical tooth surface contact on the vibration response. Through the dynamic analysis of the gear transmission system, Endo [14] pointed out that the change of meshing stiffness and tooth profile deviation was an important reason for the different vibration responses of the gear pair with tooth root crack defects and spalling defects. The time-varying meshing stiffness excitation and transmission error excitation in the meshing process were calculated by Parker [15], and the dynamic response of the gear pair at different speeds and torques was simulated by the finite element method (FEM). The dynamic model of the gear pair was used by Vaishya M and Singh R [16] to study the nonlinear dynamic response of the gear pair considering tooth surface friction. The Blok flash temperature theory and the thermal deformation equation were used by Xu [17] in the process of establishing the model, and the relationship between the wear of the high-speed gear in the wind turbine gearbox and the nonlinear dynamics was revealed.

The rolling bearing is used as a supporting component to guide the rotation of the shaft in the gearbox, so as to ensure the smooth operation of the entire equipment, and it also has an important impact on the vibration characteristics of the transmission system [18,19]. In order to completely obtain the real-time transient response of the bearing, the relative sliding and lubricating traction were considered by Gupta [20], then the dynamic model of rolling bearings was established, and the dynamic program was written in FORTAN language. Based on Gupta's model, the localized defect, variations in additional clearance, Hertzian contact stiffness, and contact load were added by Niu [21] into the dynamic model, then the dynamic response of the bearing was investigated. However, this dynamic model is very complex, and it is not easy to converge in numerical solution, which makes it difficult to obtain effective promotion and application. Therefore, the simplified dynamic model of bearings has been proposed by a large number of researchers [22,23]. Patil [24,25] established a simplified dynamic model of deep groove ball bearings with single-point and multi-point local faults, and studied the influence of defect types and fault degrees on the vibration response. Based on the Lagrangian equations, the analysis model of the rolling bearing was organized by Tandon and Choudhury [26], in which the triangular, rectangular and half-sine function were utilized to describe the shock excitation caused by localized faults with different morphologies. Patel and Upadhyay [27] studied the nonlinear vibration response of bearings with faults on raceway and the contact relationship between rolling elements and faults. With the development of computer technology, the explicit dynamic finite element model provides an effective way to simulate the internal running state of the bearing. The component of the bearing was regarded by Singh as a flexible body [28,29], and a two-dimensional finite element model of the rolling bearing with localized failure on the outer raceway was established. Through this model, the dynamic contact force between the roller and raceway can be obtained.

In the above-mentioned research, it can be seen that the dynamic research on gear pairs and bearings has been comparatively mature, and a large number of research results have been obtained. Nonetheless, in order to simplify the dynamic model, most of the research objects selected by researchers are focused on a single gear pair system or bearing system, which are all part of the gearbox, the components in the transmission system are split. Moreover, in the rare dynamic model of the gearbox, the gear pair and the bearing are considered to rotate independently, the excitation sources of the gear pair and the bearing are set to not interfere with each other, and the vibration transmission and coupling relationship between components are severely weakened, which leads to a large difference between the numerical solution of the established model and the vibration response obtained from the experimental test. Therefore, the mathematical model needs to be improved and updated to attain a clearer understanding of the vibration generation mechanism of the gearbox.

To this end, a modified dynamic model of the gearbox is established in this paper, in which the potential energy method is used to determine the meshing stiffness of the gear pair, the contact force between the bearing roller and the raceway is computed using the point contact model in the Hertz theory. The mutual interference of the excitation source of the gear pair and the bearing is given by the gyroscopic motion of the shaft, which is caused by the asynchronous vibration of the supporting bearing inner rings on both sides of the shaft, then the coupling relationship between components in the gearbox can be determined using this method. The interference between the component and vibration responses of the gearbox are further explored using the established mathematical model, and the obtained results are confirmed by experiments, which can be used to guide the fault diagnosis of the gearbox and provide substantial theoretical support for engineering practice.

2. Dynamic model of the gearbox

2.1. Model simplification

In order to prevent excessive complexity of the dynamic model, the necessary assumptions need to be made when constructing the model. In these assumptions, only some important influencing factors are discussed, and other minor contradictions are ignored, as follows:

1. The shaft is rigid, its bending deformation is not considered;
2. The axial displacements of gear pairs and bearings are ignored;
3. The lumped mass method is used to model the component, and the contact between the components is simplified as a spring-damper system;
4. Factors such as temperature and lubrication are not considered.

2.2. Dynamic model of the gearbox

On the basis of these assumptions, as shown in Figure 1, a model with 36 DOFs of the gearbox is built. The dynamic equations are [30,31]:

Preprints (www.preprints.org) | NOT PEER-REVIEWED | Posted: 14 June 2022 doi:10.20944/preprints202206.0191.v1

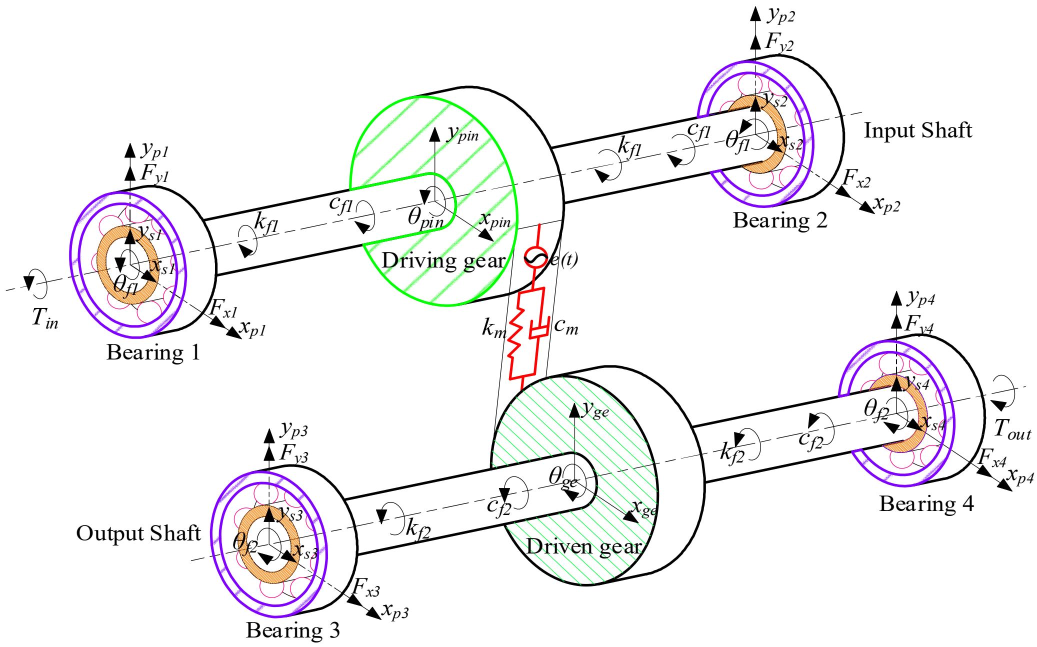

Figure 1. Dynamic model of the gearbox.

$$
\begin{cases}
I_{f1}\ddot{\theta}_{f1} + c_{f1}(\dot{\theta}_{f1} - \dot{\theta}_{pin}) + k_{f1}(\theta_{f1} - \theta_{pin}) = T_{in} \\
m_{s1}\ddot{x}_{s1} + c_{sx1}(\dot{x}_{s1} - \dot{x}_{pin}) + k_{sx1}(x_{s1} - x_{pin}) + F_{x1} = 0 \\
m_{s1}\ddot{y}_{s1} + c_{sy1}(\dot{y}_{s1} - \dot{y}_{pin}) + k_{sy1}(y_{s1} - y_{pin}) + F_{y1} = 0 \\
m_{p1}\ddot{x}_{p1} + c_{px1}\dot{x}_{p1} + k_{px1}x_{p1} - F_{x1} = 0 \\
m_{p1}\ddot{y}_{py1} + (c_{py1} + c_{r1})\dot{y}_{p1} + (k_{py1} + k_{r1})y_{p1} - k_{r1}y_{r1} - c_{r1}\dot{y}_{r1} - F_{y1} = 0 \\
m_{r1}\ddot{y}_{r1} + c_{r1}(\ddot{y}_{r1} - \dot{y}_{p1}) + k_{r1}(y_{r1} - y_{p1}) = 0 \\
I_{pin}\ddot{\theta}_{pin} - c_{f1}(\dot{\theta}_{f1} - \dot{\theta}_{pin}) - k_{f1}(\theta_{f1} - \theta_{pin}) = -R_{pin}F_M \\
m_{pin}\ddot{x}_{pin} + c_{sx1}(\dot{x}_{pin} - \dot{x}_{s1}) + c_{sx2}(\dot{x}_{pin} - \dot{x}_{s2}) + k_{sx1}(x_{pin} - x_{s1}) + k_{sx2}(x_{pin} - x_{s2}) = 0 \\
m_{pin}\ddot{y}_{pin} + c_{sy1}(\dot{y}_{pin} - \dot{y}_{s1}) + c_{sy2}(\dot{y}_{pin} - \dot{y}_{s2}) + k_{sy1}(y_{pin} - y_{s1}) + k_{sy2}(y_{pin} - y_{s2}) = F_M \\
m_{s2}\ddot{x}_{s2} + c_{sx2}(\dot{x}_{s2} - \dot{x}_{pin}) + k_{sx2}(x_{s2} - x_{pin}) + F_{x2} = 0 \\
m_{s2}\ddot{y}_{s2} + c_{sy2}(\dot{y}_{s2} - \dot{y}_{pin}) + k_{sy2}(y_{s2} - y_{pin}) + F_{y2} = 0 \\
m_{p2}\ddot{x}_{p2} + c_{px2}\dot{x}_{p2} + k_{px2}x_{p2} - F_{x2} = 0 \\
m_{p2}\ddot{y}_{py2} + (c_{py2} + c_{r2})\dot{y}_{p2} + (k_{py2} + k_{r2})y_{p2} - k_{r2}y_{r2} - c_{r2}\dot{y}_{r2} - F_{y2} = 0 \\
m_{r2}\ddot{y}_{r2} + c_{r2}(\dot{y}_{r2} - \dot{y}_{p2}) + k_{r2}(y_{r2} - y_{p2}) = 0 \\
m_{s3}\ddot{x}_{s3} + c_{sx3}(\dot{x}_{s3} - \dot{x}_{ge}) + k_{sx3}(x_{s3} - x_{ge}) + F_{x3} = 0 \\
m_{s3}\ddot{y}_{s3} + c_{sy3}(\dot{y}_{s3} - \dot{y}_{ge}) + k_{sy3}(y_{s3} - y_{ge}) + F_{y3} = 0 \\
m_{p3}\ddot{x}_{p3} + c_{px3}\dot{x}_{p3} + k_{px3}x_{p3} - F_{x3} = 0 \\
m_{p3}\ddot{y}_{p3} + (c_{py3} + c_{r3})\dot{y}_{p3} + (k_{sp3}+k_{r3})y_{p3} - k_{r3}y_{r3} - c_{r3}\dot{y}_{r3} - F_{y3} = 0 \\
m_{r3}\ddot{y}_{r3} + c_{r3}(\dot{y}_{r3} - \dot{y}_{p3}) + k_{r3}(y_{r3} - y_{p3}) = 0 \\
I_{ge}\ddot{\theta}_{ge} - c_{f2}(\dot{\theta}_{f2} - \dot{\theta}_{ge}) - k_{f2}(\theta_{f2} - \theta_{ge}) = R_{ge}F_M \\
m_{ge}\ddot{x}_{ge} + c_{sx3}(\dot{x}_{ge} - \dot{x}_{s3}) + c_{sx4}(\dot{x}_{ge} - \dot{x}_{s4}) + k_{sx3}(x_{ge} - x_{s3}) + k_{sx4}(x_{ge} - x_{s2}) = 0 \\
m_{ge}\ddot{y}_{ge} + c_{sy3}(\dot{y}_{ge} - \dot{y}_{s3}) + c_{sy4}(\dot{y}_{ge} - \dot{y}_{s4}) + k_{sy3}(y_{ge} - y_{s3}) + k_{sy4}(y_{ge} - y_{s4}) = 0 \\
m_{s4}\ddot{x}_{s4} + c_{sx4}(\dot{x}_{s4} - \dot{x}_{ge}) + k_{sx4}(x_{s4} - x_{ge}) + F_{x4} = 0 \\
m_{s4}\ddot{y}_{s4} + c_{sy4}(\dot{y}_{s4} - \dot{y}_{ge}) + k_{sy4}(y_{s4} - y_{ge}) + F_{y4} = 0 \\
m_{p4}\ddot{y}_{p4} + (c_{px4} + c_{r4})\dot{y}_{p4} + (k_{px4} + k_{r4})y_{p4} - k_{r4}y_{r4} - c_{r4}\dot{y}_{r4} - F_{y4} = 0 \\
m_{r4}\ddot{y}_{r4} + c_{r4}(\dot{y}_{r4} - \dot{y}_{p4}) + k_{r4}(y_{r4} - y_{p4}) = 0 \\
I_{f2}\ddot{\theta}_{f2} + c_{f2}(\dot{\theta}_{f2} - \dot{\theta}_{ge}) + k_{f2}(\theta_{f2} - \theta_{ge}) = -T_{out}
\end{cases} \tag{1}
$$

Where, $\boldsymbol{m_{pj}}, \boldsymbol{m_{sj}}, \boldsymbol{m_{rj}}, \boldsymbol{m_{pin}}$ and $\boldsymbol{m_{ge}}$ are the mass of the bearing outer ring, inner ring, resonator, driving gear and driven gear; $\boldsymbol{I_{f1}}, \boldsymbol{I_{f2}}, \boldsymbol{I_{pin}}$ and $\boldsymbol{I_{ge}}$ represent the inertia moment of the input shaft, output shaft, driving gear and driven gear; $\boldsymbol{\theta_{pin}}, \boldsymbol{\theta_{ge}}, \boldsymbol{\theta_{f1}}$ and $\boldsymbol{\theta_{f2}}$

represent the inertia moment of the driving gear, driven gear, input shaft and output shaft; $\boldsymbol{k_{pxj}}, \boldsymbol{k_{pyj}}, \boldsymbol{k_{sxj}}, \boldsymbol{k_{syj}}$ and $\boldsymbol{k_{ryj}}$ are the support stiffness of outer rings, inner rings and resonators; $\boldsymbol{c_{pxj}}, \boldsymbol{c_{pyj}}, \boldsymbol{c_{sxj}}, \boldsymbol{c_{syj}}$ and $\boldsymbol{c_{ryj}}$ are the support damping of outer rings, inner rings and resonators; $\boldsymbol{x_{pj}}, \boldsymbol{x_{sj}}, \boldsymbol{x_{pin}}$ and $\boldsymbol{x_{ge}}$ are the displacement of outer rings, inner rings, driving gear, and driven gear in x direction; $\boldsymbol{y_{pj}}, \boldsymbol{y_{sj}}, \boldsymbol{y_{pin}}, \boldsymbol{y_{ge}}$ and $\boldsymbol{y_{rj}}$ are the displacement in y direction; $\boldsymbol{R_{pin}}$ and $\boldsymbol{R_{ge}}$ are the radius of the driving gear base circle and driven gear base circle; $\boldsymbol{T_{in}}$ and $\boldsymbol{T_{out}}$ represent the motor torque and load torque. $\boldsymbol{F_M}$ is the meshing force of the gear pair; $\boldsymbol{F_{xj}}$ and $\boldsymbol{F_{yj}}$ represent the nonlinear contact force between the bearing raceway and rollers.

2.3. Model of the ball bearing

The simplified model of the ball bearing is established, as shown in Figure 2. $\boldsymbol{F_{xj}}$ and $\boldsymbol{F_{yj}}$ can be calculated according to the point contact model in the Hertz theory [32]. It should be noted that the subscript $\boldsymbol{j}$ is the serial number of the bearing $(\boldsymbol{j} = \mathbf{1}, \mathbf{2}, \mathbf{3}, \mathbf{4})$, which means the *j-th* bearing, and the subscript $\boldsymbol{i}$ is the serial number of the roller $(\boldsymbol{i} = \mathbf{1}, \mathbf{2}\ldots \boldsymbol{n_{bj}})$, which means the *i-th* roller in the *j-th* bearing.

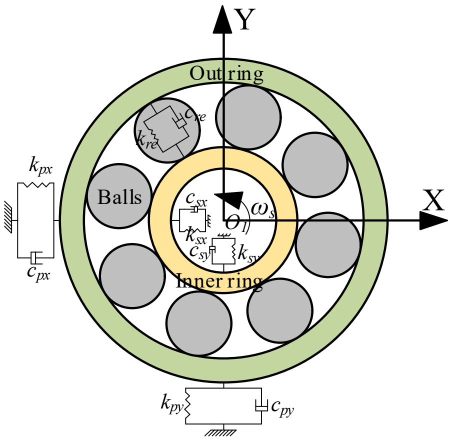

Figure 2. Model of the ball bearing.

$$\begin{cases} F_{xj} = k_{rej} \sum_{i=1}^{n_{bj}} \left(\gamma_{ij} \varepsilon_{ij}^{n} \cos \theta_{ij}\right) \\ F_{yj} = k_{rej} \sum_{i=1}^{n_{bj}} \left(\gamma_{ij} \varepsilon_{ij}^{n} \sin \theta_{ij}\right) \end{cases} \tag{2}$$

Where, $\boldsymbol{n_{bj}}$ represents the total number of rollers; $\boldsymbol{k_{rej}}$ is the equivalent stiffness between the ball and bearing raceway, the power exponent $\boldsymbol{n}$ is 1.5 when the ball acts as a roller.

$$\gamma_{ij} = \begin{cases} 1 & \delta_i > 0 \\ 0 & \text{else} \end{cases} \tag{3}$$

$\boldsymbol{\theta_{ij}}$ indicates the azimuth of the roller, which is emulated as:

$$\theta_{ij} = \frac{2\pi(i-1)}{n_{bj}} + \left(1 - \frac{d_{bj}}{d_{mj}}\right)\frac{w_{sj}}{2} t + \theta_{0ij} \tag{4}$$

Where, $\boldsymbol{d_{bj}}$ is the diameter of balls; $\boldsymbol{d_{mj}}$ is the pitch diameter of the bearing; $\boldsymbol{\theta_{0ij}}$ is the initial phase of the bearing cage; $\boldsymbol{w_{sj}}$ is the angular speed of bearing inner rings.

$\boldsymbol{\varepsilon_{ij}}$ is the contact deformation between raceways and balls, which can be expressed by the displacement of the bearing component.

$$\varepsilon_{ij} = \left(y_{sj} - y_{pj}\right) \sin \theta_{ij} + \left(x_{sj} - x_{pj}\right) \cos \theta_{ij} - c_{bwj} \tag{5}$$

Where, $\boldsymbol{c_{bwj}}$ represents the clearance of the *j-th* bearing.

Preprints (www.preprints.org) | NOT PEER-REVIEWED | Posted: 14 June 2022 doi:10.20944/preprints202206.0191.v1

The rotational frequency $\boldsymbol{f_{r1}}$ and $\boldsymbol{f_{r2}}$ of the high-speed shaft and the low-speed shaft can be calculated as:

$$\begin{cases} f_{r1} = \dfrac{n_{high}}{60} \\ f_{r2} = \dfrac{n_{low}}{60} = f_{r1} \cdot \dfrac{z_1}{z_2} \end{cases} \tag{6}$$

Where, $\boldsymbol{z_1}$ and $\boldsymbol{z_2}$ are the teeth number of the driving gear and the driven gear, $\boldsymbol{n_{high}}$ and $\boldsymbol{n_{low}}$ are the rotational speeds of the high-speed shaft and the low-speed shaft.

Therefore, the pass frequency $\boldsymbol{f_{oj}}$ of the bearing outer raceway is [33]:

$$f_{oj} = 0.5 f_r (1 - \frac{d_{bj}}{d_{mj}}) \tag{7}$$

2.4. The model of the coupling relationship between the gear pair and the bearing in the gearbox

In the gearbox, the gyroscopic motion of the shaft is caused by asynchronous vibration of the bearing inner rings on both sides of the shaft, as shown in Figure 3. Then, the center distance error and misalignment angle of the gear pair are generated. Using this method, the coupling relationship between the gear pair and the bearing can be determined.

In Figure 3, $\boldsymbol{L}$ is the length of the shaft, and $\boldsymbol{a'}$ is the actual center distance of the gear pair. It can be seen that the misalignment angle $\boldsymbol{\theta}$ between the two shafts is the angle between the vector $\overrightarrow{\boldsymbol{AC}}$ and the vector $\overrightarrow{\boldsymbol{DF}}$, the length of vector $\overrightarrow{\boldsymbol{BE}}$ is the actual center distance of the gear pair, and the following expression is satisfied.

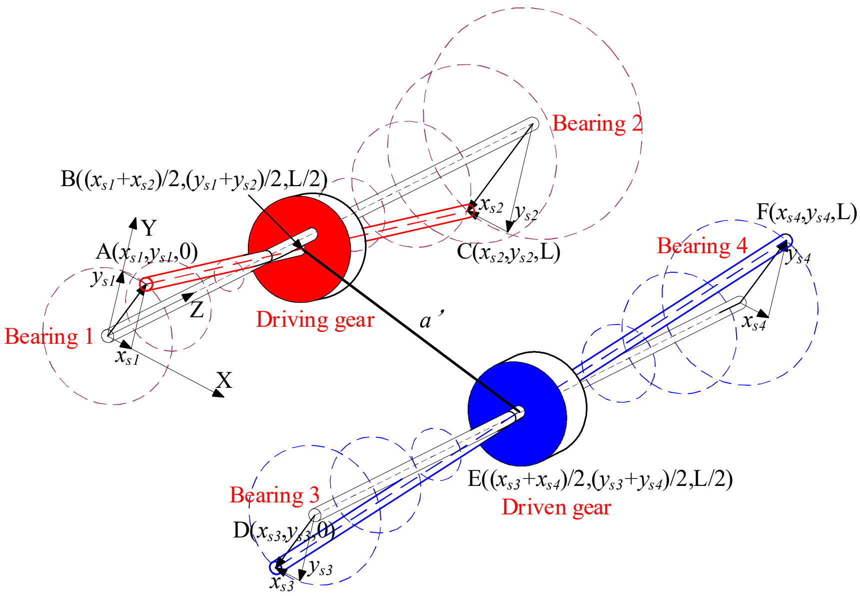

Figure 3. The model of the coupling relationship between the gear pair and the bearing in the gearbox.

$$a' = |\overrightarrow{BF}| = \sqrt{\left(\frac{x_{s1}+x_{s2}}{2} - \frac{x_{s3}+x_{s4}}{2}\right)^2 + \left(\frac{y_{s1}+y_{s2}}{2} - \frac{y_{s3}+y_{s4}}{2}\right)^2} \tag{8}$$

$$\theta = \angle(\overrightarrow{\mathrm{AC}}, \overrightarrow{\mathrm{DF}}) = \mathrm{acrcos}\frac{(x_{s1}+x_{s2})(x_{s3}+x_{s4}) + (y_{s1}+y_{s2})(y_{s3}+y_{s4}) + L^2}{\sqrt{[(x_{s1}+x_{s2})^2 + (y_{s1}+y_{s2})^2 + L^2] \cdot [(x_{s3}+x_{s4})^2 + (y_{s3}+y_{s4})^2 + L^2]}} \tag{9}$$

$$\Delta a = a' - a \tag{10}$$

Where, $\boldsymbol{a}$ is the ideal center distance of the gear pair under standard installation, $\boldsymbol{\Delta a}$ is the center distance error.

2.5. Model of the gear pair and meshing stiffness

When the gear pair is operated under the condition of misalignment and center distance error, the meshing force between the gear teeth will be deflected, as shown in Figure 3(a) and Figure 3(b). Then the meshing stiffness of the gear pair can be quantified using the potential energy method [34], and the cantilever beam model is shown as Figure 3(c).

In Figure 3, $\boldsymbol{F}$ represents the equivalent concentrated force of the meshing force $\boldsymbol{F_M}$, $\boldsymbol{F_a}$ and $\boldsymbol{F_b}$ can be obtained after the meshing force $\boldsymbol{F}$ is decomposed, $\boldsymbol{F_t}$ is the normal force acting on the tooth surface, $\boldsymbol{W}$ is the width of the gear teeth, and $\boldsymbol{\alpha_1}$ is the pressure angle at the actual meshing point, $\boldsymbol{\alpha_2}$ represents the half of the center angle corresponding to a gear tooth, $\boldsymbol{h_x}$ represents the distance between the meshing point and the center line *OP*, $\boldsymbol{R}$ and $\boldsymbol{R_a}$ represent the radius of the pitch and addendum circles.

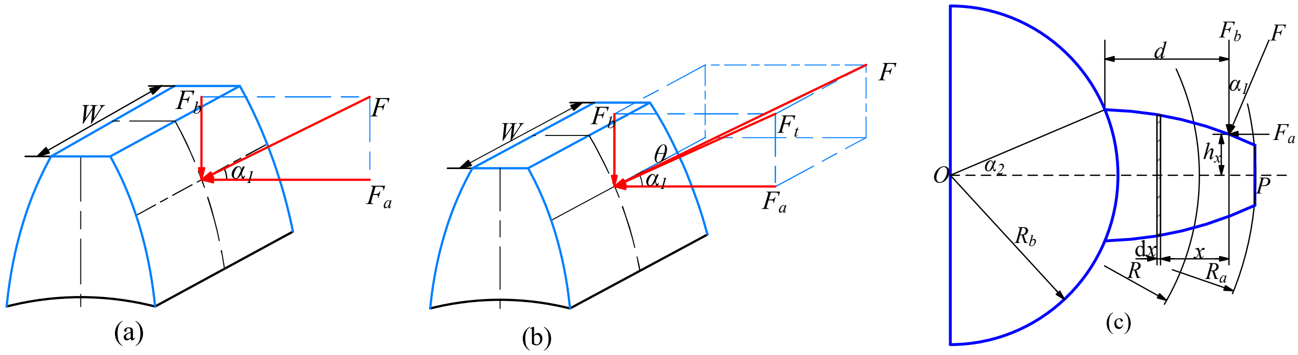

Figure 3. Force decomposition: (a) Alignment; (b) Misalignment; (c) Cantilever beam model.

Bending deformation energy $\boldsymbol{U_b}$:

$$U_b = \int_0^d \frac{[-F_a h + F_b(d-x)]^2}{2EI_s} \mathrm{d}x = \frac{F^2}{2k_b} \tag{11}$$

Shear deformation energy $\boldsymbol{U_s}$:

$$U_s = \int_0^d \frac{(1.2F_b)^2}{2GA_s} \mathrm{d}x = \frac{F^2}{2k_s} \tag{12}$$

Radial compression deformation energy $\boldsymbol{U_a}$:

$$U_a = \int_0^d \frac{F_a^2}{2EA_s} \mathrm{d}x = \frac{F^2}{2k_a} \tag{13}$$

As shown in Figure 4, when there is a misalignment error on the gear pair, F_t will no longer be uniformly distributed, but will show the characteristics of parabolic distribution [35]. Since the vibration of the gearbox in the x-direction is only excited by the contact force of the bearing, the vibration amplitude in this direction is much smaller than that in the y-direction. Therefore, only the misalignment in the y direction is considered, and the meshing area of the gear is still parallel to the centerline of the shaft, which can also avoid the tediousness of using the slicing method to obtain meshing stiffness.

The torsional deformation of the gear teeth is caused due to uneven force on the gear teeth, so the torsional stiffness $\boldsymbol{k_\tau}$ of the gear pair is generated, and the torsion moment is $\boldsymbol{T = F_t \cdot t}$. Similarly, the potential energy method is used to establish a calculation model for the torsional stiffness [36].

Torsional deformation energy $\boldsymbol{U_\tau}$:

$$U_\tau = \int_0^d \frac{(F_t \cdot t)^2}{2GI_{px}} \mathrm{d}x = \frac{F^2}{2k_\tau} \tag{14}$$

Where, $\boldsymbol{I_s}, \boldsymbol{A_s}$ and $\boldsymbol{I_{px}}$ represent the inertia moment, the cross-sectional area and polar inertia moment of the gear tooth, which can be calculated as:

$$\begin{cases} A_s = 2h_x W \\ I_s = \dfrac{(2h_x W)^3}{12} \\ I_{px} = \dfrac{2h_x L}{12}(4h_x^2 + L^2) \end{cases} \tag{15}$$

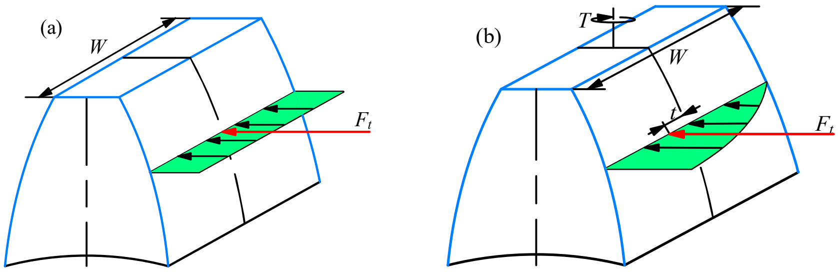

Figure 4. The distributed load of the gear pair is replaced by the concentrated load: (a) Alignment; (b) Misalignment.

According to the force decomposition of Figure 3 and Figure 4, the following equation is established:

$$\begin{cases} F_t = F\cos\theta \\ F_b = F_t\cos\alpha_1 = F\cos\theta\cos\alpha_1 \\ F_a = F_t\sin\alpha_1 = F\cos\theta\sin\alpha_1 \end{cases} \tag{16}$$

Then, the stiffness component can be obtained after simplification.

Bending stiffness $\boldsymbol{k_b}$:

$$\frac{1}{k_b} = \int_{-\alpha_1}^{\alpha_2} \frac{12\left\{1+\cos\alpha_1[(\alpha_2-\alpha)\sin\alpha-\cos\alpha] - 2\cos\alpha_1\sin^2\dfrac{\theta}{2}\begin{bmatrix}((\alpha_1+\alpha_2)\cos\alpha_1-\sin\alpha) \\ -(\cos\alpha-(\alpha_2-\alpha)\sin\alpha-\cos\alpha_2)\end{bmatrix}\right\}^2(\alpha_2-\alpha)\cos\alpha}{8EW[\sin\alpha+(\alpha_2-\alpha)\cos\alpha]^3}\mathrm{d}\alpha \tag{17}$$

Shear stiffness k_s:

$$\boldsymbol{\frac{1}{k_s} = \int_{-\alpha_1}^{\alpha_2} \frac{1.2(1+v)(\alpha_2-\alpha)\cos\alpha\cos^2\alpha_1\cos^2\theta}{EW[\sin\alpha+(\alpha_2-\alpha)\cos\alpha]}}\mathrm{d}\boldsymbol{\alpha} \tag{18}$$

Radial compression stiffness $\boldsymbol{k_a}$:

$$\frac{1}{k_a} = \int_{-\alpha_1}^{\alpha_2} \frac{(\alpha_2-\alpha)\cos\alpha\sin^2\alpha_1\cos^2\theta}{2EW[\sin\alpha+(\alpha_2-\alpha)\cos\alpha]}\mathrm{d}\alpha \tag{19}$$

Torsional stiffness $\boldsymbol{k_\tau}$:

$$\frac{1}{k_\tau} = \int_{-\alpha_1}^{\alpha_2} \frac{3L(1+v)(\alpha_2-\alpha)\cos^2\alpha_1\cos^2\theta\cos\alpha}{16E[\sin\alpha+(\alpha_2-\alpha)\cos\alpha]\{4R_b^2[\sin\alpha+(\alpha_2-\alpha)\cos\alpha]^2+W^2\}}\mathrm{d}\alpha \quad 20)$$

Similarly, the meshing stiffness of the gear pair is also affected by the actual center distance. According to the meshing principle of the gear pair, equation (21) is given as:

$$\alpha' = \arccos\left(\frac{a\cos\alpha}{a+\Delta a}\right) \tag{21}$$

Where, α' is the actual pressure angle of the gear pair. The meshing stiffness calculation model of the gear pair under the coupling effect of the center distance error and misalignment angle can be determined by replacing $\boldsymbol{\alpha}$ in equations (17-20) with $\boldsymbol{\alpha'}$.

The nonlinearity of the meshing force $\boldsymbol{F_M}$ of the gear pair is considered, which mainly comes from the elastic meshing force $\boldsymbol{F_k}$ and the viscous meshing force $\boldsymbol{F_c}$, as follows [37]:

$$\begin{cases} F_M = F_k + F_c \\ F_k = k_t\left(R_{pin}\theta_{pin} - R_{ge}\theta_{ge} - y_{pin} + y_{ge} - e_t\right) \\ F_c = c_t\left(R_{pin}\dot{\theta}_{pin} - R_{ge}\dot{\theta}_{ge} - \dot{y}_{pin} + \dot{y}_{ge} - \dot{e}_t\right) \end{cases} \tag{21}$$

Where, k_t and c_t are comprehensive meshing stiffness and meshing damping.

e_t is the transmission error and can be simulated by the trigonometric function [38].

$$e_t = e_o + e_m \sin\left(2\pi f_m t + \varphi_o\right) \tag{23}$$

Where, f_m is the meshing frequency, e_m and e_o represent the fluctuation and average error.

$$f_m = z_1 f_{r1} = z_2 f_{r2} \tag{24}$$

The model in Ref 39 and Ref 40 is used to calculate the matrix deformation stiffness k_f and the Hertzian contact stiffness k_h of the gear pair, then the comprehensive meshing stiffness of the gear pair can be obtained as [41]:

$$\frac{1}{k_t} = \begin{cases} \sum_{i=1}^{2}\left(\frac{1}{k_{b1,i}} + \frac{1}{k_{s1,i}} + \frac{1}{k_{a1,i}} + \frac{1}{k_{h,i}} + \frac{1}{k_{f1,i}} + \frac{1}{k_{s2,i}} + \frac{1}{k_{f2,i}} + \frac{1}{k_{a2,i}} + \frac{1}{k_{b2,i}} + \frac{1}{k_{\tau1,i}} + \frac{1}{k_{\tau2,i}}\right) & \text{double tooth} \\ \frac{1}{k_{s1}} + \frac{1}{k_{b1}} + \frac{1}{k_{a1}} + \frac{1}{k_h} + \frac{1}{k_{f1}} + \frac{1}{k_h} + \frac{1}{k_{f2}} + \frac{1}{k_{b2}} + \frac{1}{k_{a2}} + \frac{1}{k_h} + \frac{1}{k_{s2}} + \frac{1}{k_{\tau1}} + \frac{1}{k_{\tau2}} & \text{single tooth} \end{cases} \tag{25}$$

3. Results and experimental verification

The main parameters of the gear pair and bearing types are listed in Table 1, and the parameters in the dynamic model are shown in Table 2. The established dynamic equations of the gearbox are solved using the $Runge-Kutta$ method, and a flow chart of the whole process is configured and provided in Figure 5. The total working time and working step are set to 2s and 10^{-5}s, the initial state of the system is set to 0. After the numerical solution is obtained, the vibration acceleration $\ddot{y}_{b1}$ of the bearing 1 resonator is extracted as the analysis signal, and the frequency-domain response of the system can be obtained through the Fast Fourier Transform (*FFT*).

Table 1. The main parameters of the gear pair and bearing types.

Parameter/(unit)	Driving gear	Driven gear	Bearing	Types
Modulus *m/mm*	2.5	2.5	Bearing 1	6304
Number of teeth *z*	23	81	Bearing 2	6304
Pressure Angle *α*/(°)	20	20	Bearing 3	6308
Tooth width *W/mm*	26	26	Bearing 4	6308
Young's modulus *E/GPa*	206	206	-	-
Poisson's ratio *v*	0.3	0.3	-	-

After the dynamic equation of the gearbox is solved, the numerical solution can be obtained. Then the center distance error $\Delta\boldsymbol{a}$, the misalignment angle $\boldsymbol{\theta}$ and the time-varying meshing stiffness $\boldsymbol{k_t}$ of the gear pair are extracted, and the results are shown in Figure 6. The center distance error $\Delta\boldsymbol{a}$ and misalignment angle $\boldsymbol{\theta}$ of the gear pair are shown in Figure 6(a) and Figure 6(b) respectively, it can be seen that during the operation of the gearbox, $\Delta\boldsymbol{a}$ and $\boldsymbol{\theta}$ are changed periodically. There are 23 local peaks on the curve in one revolution of the high-speed shaft, which is consistent with the teeth number of the driving gear. This shows that the $\Delta\boldsymbol{a}$ and $\boldsymbol{\theta}$ between the high-speed shaft and the low-speed shaft are mainly motivated by the meshing behavior of the gear pair, the asynchronous vibration of the support bearing inner ring is aggravated, which causes the eccentricity and misalignment of the shaft. Also, the meshing behavior of the gear pair is affected by the actual center distance and misalignment, which is equivalent to the formation of a complete control closed loop. In this closed loop, the meshing behavior of the gear pair

Preprints (www.preprints.org) | NOT PEER-REVIEWED | Posted: 14 June 2022 doi:10.20944/preprints202206.0191.v1

not only plays the role of emitting excitation, but also is controlled by the excitation from the closed loop. It is further explained that in the gearbox, the transmission path of vibration is closed, and there is a strong coupling relationship between the gear pair and the bearing.

Table 2. Parameters of the gearbox model.

Parameters	Values	Parameters	Values
Inertia moment of input shaft $I_{f1}/(kg \cdot m^2)$	0.0021	Torsional stiffness of shaft k_{f1}, k_{f2} $/(Nm/rad)$	$4.4e^{5}$
Inertia moment of driving gear $I_{pin}/(kg \cdot m^2)$	$4.365e^{-4}$	Torsional damping of shaft $c_{f1}, c_{f2}/(Nms/rad)$	$5e^{5}$
Inertia moment of driven gear $I_{ge}/(kg \cdot m^2)$	$8.362e^{-4}$	Stiffness of bearings $k_{sj}, k_{pj}, k_{rj}/(N/m)$	$6.56e^{7}$
Inertia moment of output shaft $I_{f2}/(kg \cdot m^2)$	0.0105	Damping of bearings $c_{sj}, c_{pj}, c_{rj}/(Ns/m)$	$1.8e^{5}$
Load (N/m)	30	Mass of the coupling housing m_{pin}/kg	1
Average transmission error e_o/m	$3e^{-5}$	Mass of driving gear m_{pin}/kg	0.96
Transmission fluctuation range e_m/m	$2e^{-5}$	Mass of driven gear m_{ge}/kg	2.88
Rotation frequency of input shaft f_{r1}/Hz	30	length of shaft L/mm	205

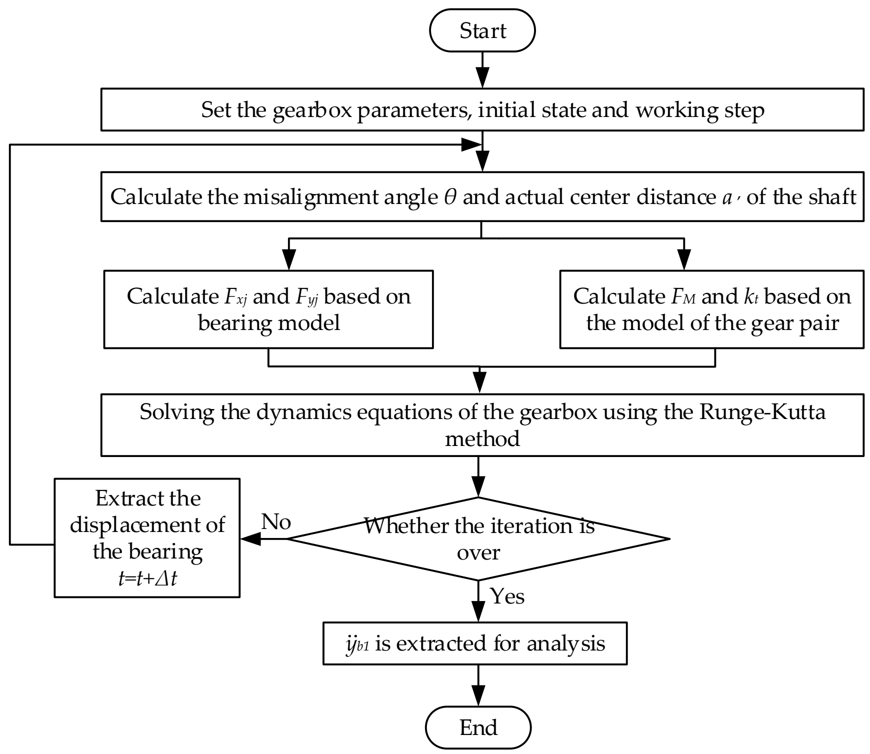

Figure 5. The flow chart for the whole process.

Similarly, the bearing also has an influence on $\Delta\boldsymbol{a}$ and $\boldsymbol{\theta}$ of the shaft, which is mainly reflected in the amplitude modulation of the passing frequency of the bearing outer raceway. It can be seen from Figure 6(a) and Figure 6(b) that $\Delta\boldsymbol{a}$ and $\boldsymbol{\theta}$ are modulated by the passing frequency $\boldsymbol{f_{o1}}$ of the bearing outer raceway. Since the gear pair is generally located at the midpoint of the shaft, it is not sensitive to the gyroscopic motion of the shaft. On the contrary, the misalignment angle is more seriously modulated by the shaft motion.

The dynamic meshing stiffness of the gear pair in the gearbox is plotted in Figure 6(c) and compared with the results from the model proposed by Sawalhi [43]. When the Sawalhi model is used to calculate the meshing stiffness of the gear pair, it is found that the meshing stiffness curve is strictly cyclically varied. In his model, only the influence of the gear pair structure on the meshing stiffness is considered, and the vibration displacement factor of the system is ignored.

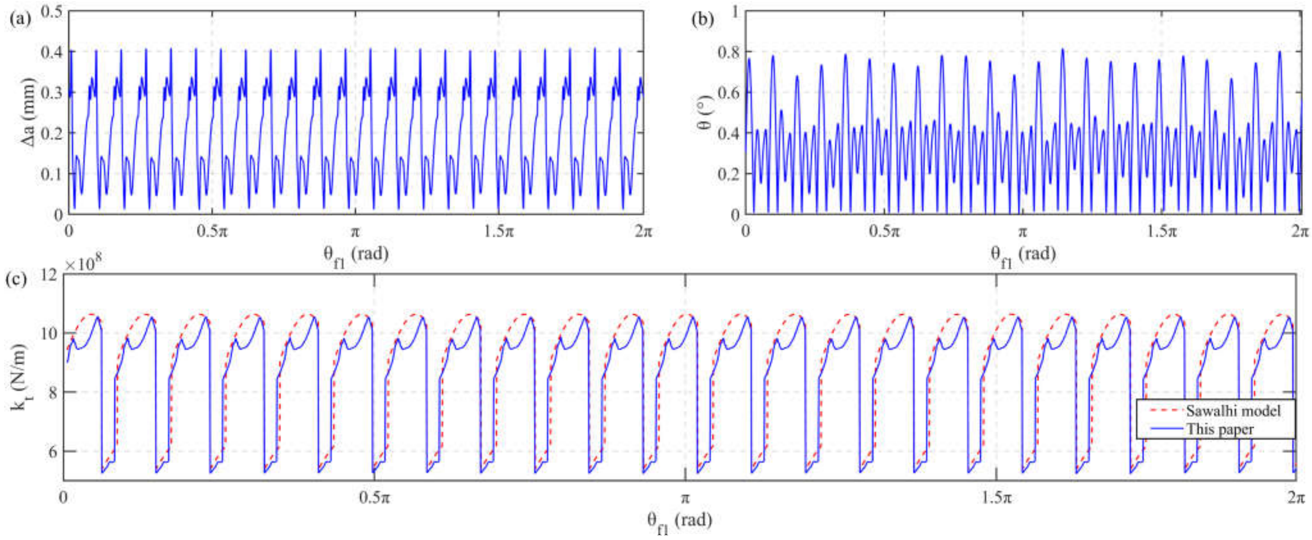

Figure 6. Internal excitation of the gearbox: (a) center distance error; (b) misalignment angle, (c) meshing stiffness of gear pair.

From the results of the model established in this paper, it is found that the meshing stiffness will be affected by the motion of the shaft and bearing, and the excitation source is increased, which leads to a decrease in the meshing stiffness compared with the results obtained by the Sawalhi model as a whole. There are more local peaks on the meshing stiffness curve, the periodicity is worse, and it also shows the characteristics of weak non-stationarity. Especially at the alternation of the single-tooth meshing interval and the double-tooth meshing interval of the gear pair, the meshing stiffness value is abruptly changed, the normal vibration of the gear pair is generated, which causes a large center distance error and misalignment angle, and maximizes the reduction in meshing stiffness. In addition, the meshing behavior of the gear pair becomes chaotic, and the length of the single and double meshing interval is changed, which is also slightly affected by the amplitude modulation of the bearing.

In order to prove that the vibration mechanism in the gearbox can be more accurately described by the model established in this paper, the response obtained by the model are compared with the result from the Sawalhi model and experiment respectively.

The Experiments are carried out by using the gearbox experimental equipment modeled HD-CL-012C, which was manufactured in Wuxi Houde Automation Instrument Co., Ltd in China, and is shown in Figure 7. The transmission ratio of the gear pair in the gearbox is 23:81, and the bearing types are 6304 and 6308, which are purchased from NSK in Japan. The speed of the motor (ABB motors-QABP100L, 2A) is set to 1800rpm, and the load of the magnetic powder brake (FZ50Y) is selected to be 30N m. A 16-channel data collector (HD9200) and acceleration sensor (HD-YD-232) are used to measure the response of the gearbox in the plumb direction, this direction is the closest to the meshing action line of the gear pair, and the experimental error is the smallest. The measurement point is set at the bearing end cover, the sampling frequency is set to 30k Hz, and the results are shown in Figure 8.

There is no obvious shock in the time-domain signal obtained by the experimental method, which indicates that the gearbox is in good operating condition without any localized defects, and is modulated by the passing frequency of the bearing outer raceway. More effective information can be obtained in its frequency-domain response, in which the passing frequencies of the bearing outer raceway can be found, such as $f_{o1}, 2f_{o1}, 3f_{o1}...$, which verifies that the system is supported by the bearing and is also modulated by the bearing. And there are the meshing frequencies of the gear pair in the

Preprints (www.preprints.org) | NOT PEER-REVIEWED | Posted: 14 June 2022 doi:10.20944/preprints202206.0191.v1

spectrum, such as $f_m, 2f_m\ldots$, and the amplitude is relatively large, which indicates that the vibration of the gearbox is mainly caused by the meshing behavior of the gear pair. It is worth noting that on both sides of the meshing frequency, there are obvious harmonic frequencies of the gear pair, such as $f_m \pm f_{r1}, f_m \pm 2f_{r1}, 2f_m \pm f_{r1}, 2f_m \pm 2f_{r1}\ldots$ These frequency components are generated by the frequency modulation of the meshing frequency and the frequency of the rotating shaft, which further shows that the excitation source of the meshing stiffness is not only determined by its own properties, but other factors will also affect the vibration of the gear pair, so the meshing stiffness excitation is not strictly periodic and stable.

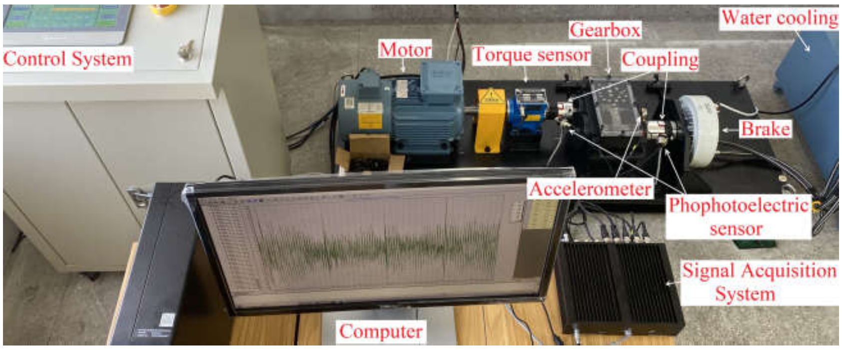

Figure 7. HD-CL-012C Gearbox Test Bench.

Similar to the experimental results, there is no obvious shock signal in the time-domain response obtained by using Sawalhi model, and the response is relatively stable, which is also affected by the amplitude modulation of the bearing. However, the main separation between this result and the experimental result is reflected in the frequency spectrum, and it is difficult to find the harmonic frequencies of the gear pair. Since the excitation of the system vibration and shaft motion on the gear pair is ignored in Sawalhi model, the generation mechanism of the harmonic frequency cannot be explained, so the real vibration mechanism of the gearbox cannot be completely and accurately described.

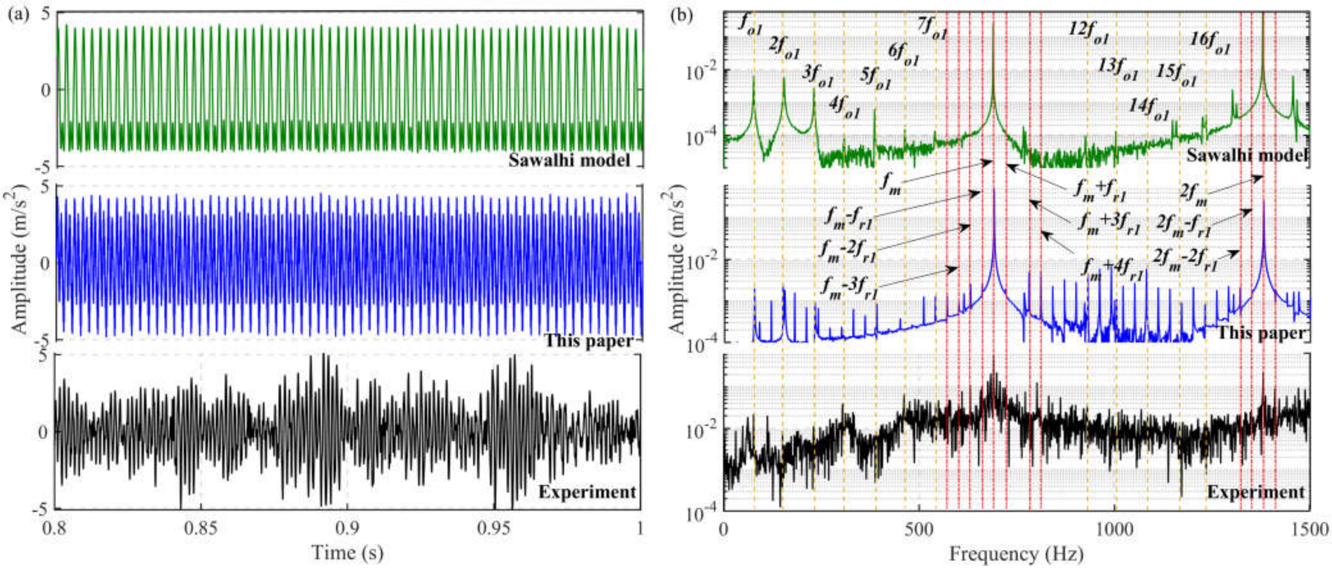

Figure 8. Vibration response of gearbox: (a) time-domain response; (b) frequency-domain response.

This problem can be perfectly explained using the dynamic equations established in this paper. The time-domain response obtained by the model established in this paper is no different from the experimental results and the results of the Sawilhi model. In the spectrum, in addition to the passing frequency of the bearing outer raceway and the meshing frequency of the gear pair, the harmonic frequencies of the gear pair are also found, such as $f_m \pm f_{r1}, f_m \pm 2f_{r1}, 2f_m \pm f_{r1}, 2f_m \pm 2f_{r1}$.... This result is highly similar to the experimental result, which can be used to explain the generation of the harmonic response and truly understand the vibration mechanism of the gearbox.

4. Discussion

The established dynamic model of the gearbox has been verified by experiments, then the vibration characteristics of the gearbox at different speeds are further discussed, which can provide theoretical reference for engineering practice and subsequent research.

The input rotational frequency $\boldsymbol{f_{r1}}$ is set to 30Hz, 40Hz, 50Hz and 60Hz, respectively. After the dynamic equation of the gearbox is solved, the internal excitation source of the gearbox is obtained as shown in Figure 9. It is found that as the rotation speed increases, the vibration amplitude of the bearing inner ring is increased, and the more severe gyroscopic motion of the transmission shaft is caused, which makes the center distance error and misalignment angle continue to increase, and the amplitude modulation of the bearing outer raceway is more obvious, as shown in Figure 9(a) and Figure 9(b). Due to the fluctuation of the center distance error curve and the misalignment angle curve, it is difficult to quantify the degree of its excitation to meshing stiffness, and these fluctuating data can be processed using the root mean square (*RMS*) in mathematical statistics, the result is shown in Table 3. It can be seen that with the increase of the gearbox speed, the RMS value of the $\Delta\boldsymbol{a}$ and $\boldsymbol{\theta}$ shows a consistent increasing trend, which further reveals that the higher the speed, the greater the excitation intensity of the bearing motion on the meshing stiffness.

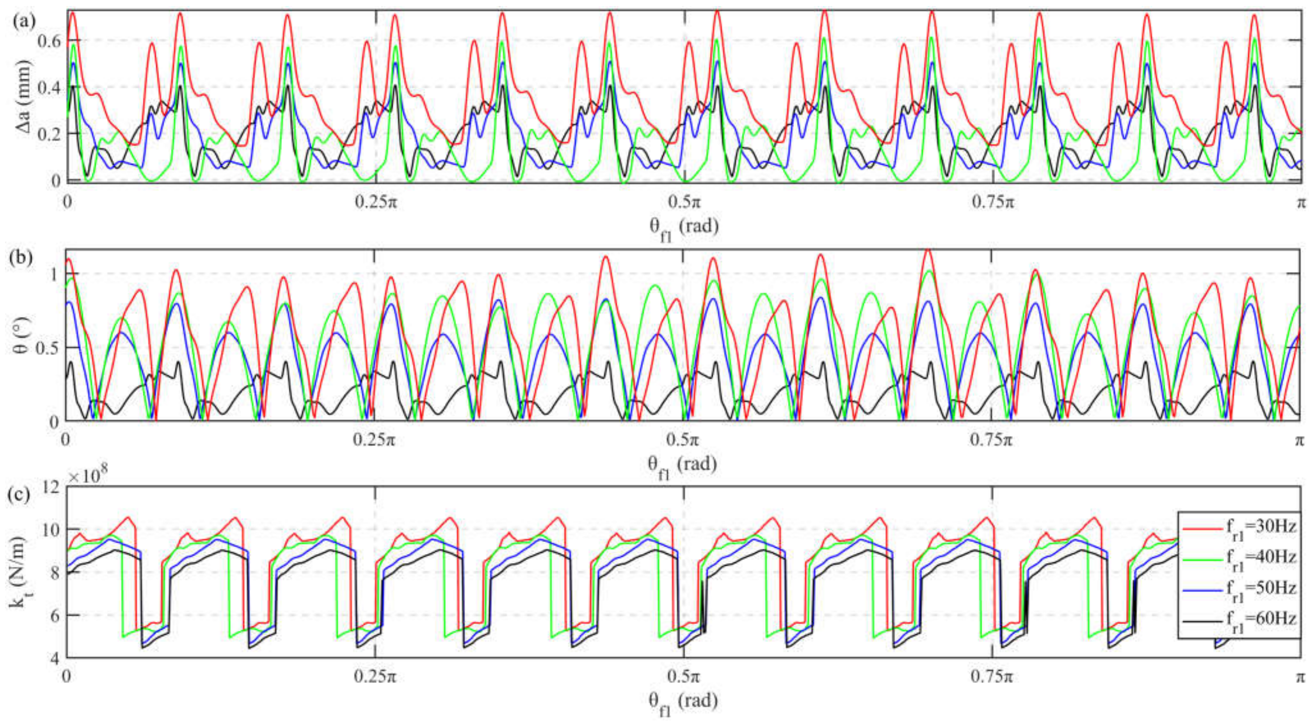

Figure 9. Excitation sources in the gearbox at different speeds: (a) center distance error; (b) misalignment angle; (c) meshing stiffness.

Figure 9(b) shows the meshing stiffness of the gear pair at different speeds. It is found that as the rotational speed increases, the meshing process of the gear pair becomes more chaotic, and the meshing stiffness value is continuously reduced as a whole. The length of the single-tooth and double-tooth meshing interval of the gear pair is changed from the original fixed value to the time-varying value. Especially when the input speed is

3600rpm, the center distance error and misalignment angle are maximized, which causes the single and double-tooth meshing interval to no longer show regular alternation. When the gear pair is driven by a single pair of gear teeth, the next pair of gear teeth that are about to enter meshing will be unexpectedly entered meshing ahead of time due to the movement of the shaft, which is easy to cause the disorder of the meshing process, and this is extremely unfavorable for the meshing process of the gear pair and the vibration of the gearbox.

Table 3. *RMS* value of center distance error and misalignment angle.

f_{r1} (Hz) / *RMS* (m/s²)	30	40	50	60
Δa	0.218	0.226	0.237	0.254
θ	0.487	0.535	0.563	0.612

The response of the gearbox at different speeds is shown in Figure 10, it is found that when the gearbox is operated at different speeds, the response is still a periodic and stable signal. As the rotational speed increases, the modulation effect of the bearing outer raceway on the response is enhanced, and the vibration amplitude of the system will be increased, as shown in Figure 10(a), which is related to the rotational speed excitation of the system.

The frequency-domain response of the gearbox can be obtained by using the *FFT*, as shown in Figure 10(b). In order to facilitate the comparison of the spectrum composition at different rotational speeds, the horizontal axis in the spectrum is transformed into the order, $\textbf{Order} = \boldsymbol{F/f_{r1}}$, where, Order represents the dimensionless rotation order, and *F* is the abscissa in the original spectrum. When the gearbox is operated at different speeds, the bearing outer raceway passing frequency and the meshing frequency of the gear pair can still be found in the spectrum, such as $\boldsymbol{f_{o1}}$, $\boldsymbol{2f_{o1}}$, $\boldsymbol{3f_{o1}}$, $\boldsymbol{f_m}$, $\boldsymbol{2f_m}$..., and these frequency amplitudes are listed in Table 4. It can be seen that in the process of increasing the speed, the fundamental frequency of $\boldsymbol{f_{o1}}$ and $\boldsymbol{f_m}$ has been increased, the amplitude of their double super harmonic $\boldsymbol{2f_{o1}}$ and $\boldsymbol{2f_m}$ is instead reduced, which means that although the vibration amplitude of the system is increased, it can make the system vibrate mainly at the fundamental frequency.

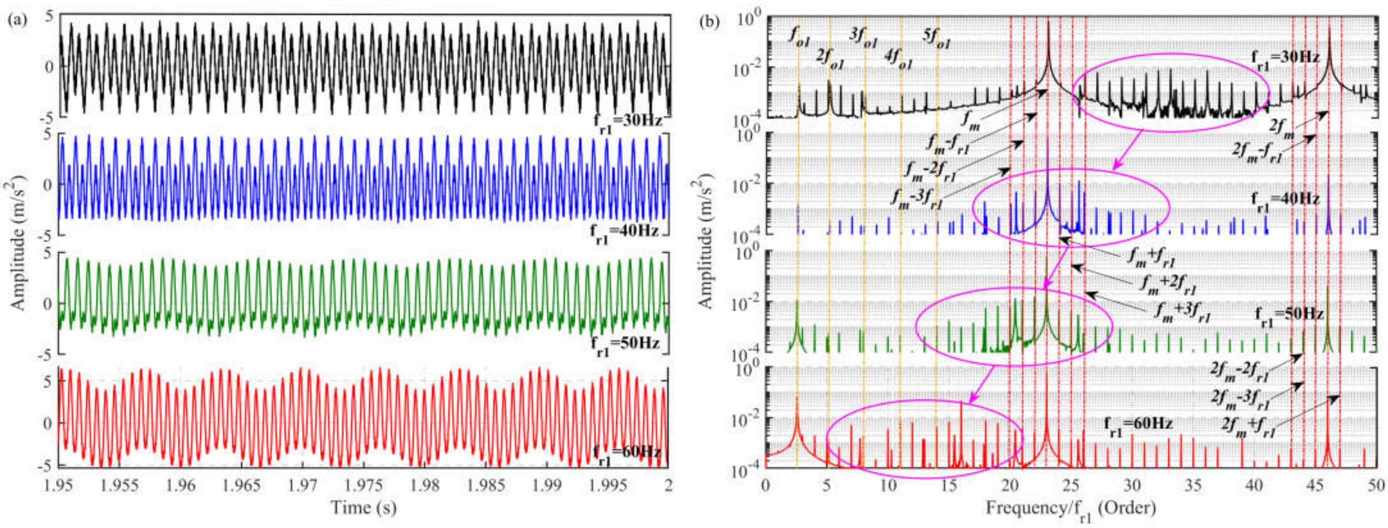

Figure 10. Response of gearbox at different speeds: (a) time-domain response; (b) frequency-domain response.

On both sides of the meshing frequency, the harmonic frequencies of the gear pair can also be found, such as $\boldsymbol{f_m \pm f_{r1}, f_m \pm 2f_{r1}, 2f_m \pm f_{r1}, 2f_m \pm 2f_{r1}}$..., and their amplitudes are continuously increased. This shows that at different speeds, the harmonic response of the gear pair can be excited, and the excitation intensity of the system vibration on the meshing behavior of the gear pair is continuously enhanced with the increase of the speed. From the distribution interval of these harmonic frequencies, as the rotation speed is increased, the harmonic frequency is advanced from the original $\boldsymbol{f_m \sim 2f_m}$ frequency range to the $\boldsymbol{0 \sim f_m}$ frequency range, which proves that as the speed increases, the harmonic frequency of the gear pair is continuously shifted to the low frequency band.

Table 4. Amplitudes of the frequency**.**

f_{r1} (Hz) / Frequency (Hz)	30	40	50	60
f_m	0.5224	0.5678	0.6066	0.6536
$2f_m$	0.4873	0.4248	0.3438	0.2824
f_{o1}	0.025	0.1253	0.1714	0.2028
$2f_{o1}$	0.0191	0.0042	0.0037	0.0017

In order to compare the operating stability of the gearbox at different speeds, the displacements in the x-direction and y-direction of the bearing 1 outer ring are extracted and drawn into the axis trace, the results are shown in Figure 11. In the axis track of the outer ring, the support role of the bearing and the shock caused by the meshing behavior of the gear pair can be easily identified. The axis track roughly presents an elliptical shape, the long axis of the ellipse is corresponding to the displacement in the y direction of the outer ring, which is excited by the Hertzian contact force of the bearing and the nonlinear meshing force of the gear pair, and the vibration amplitude caused is relatively large. The short axis of the ellipse is corresponding to the displacement in the x direction of the outer ring, and the vibration is only excited by the Hertzian contact force of the bearing, and the amplitude is relatively small. As the rotational speed increases, the axis track of the outer ring becomes more and more chaotic, which means that the excitation of the gear pair vibration is aggravated by the gyroscopic motion of the shaft, the stability of the gearbox operation becomes worse.

Preprints (www.preprints.org) | NOT PEER-REVIEWED | Posted: 14 June 2022 doi:10.20944/preprints202206.0191.v1

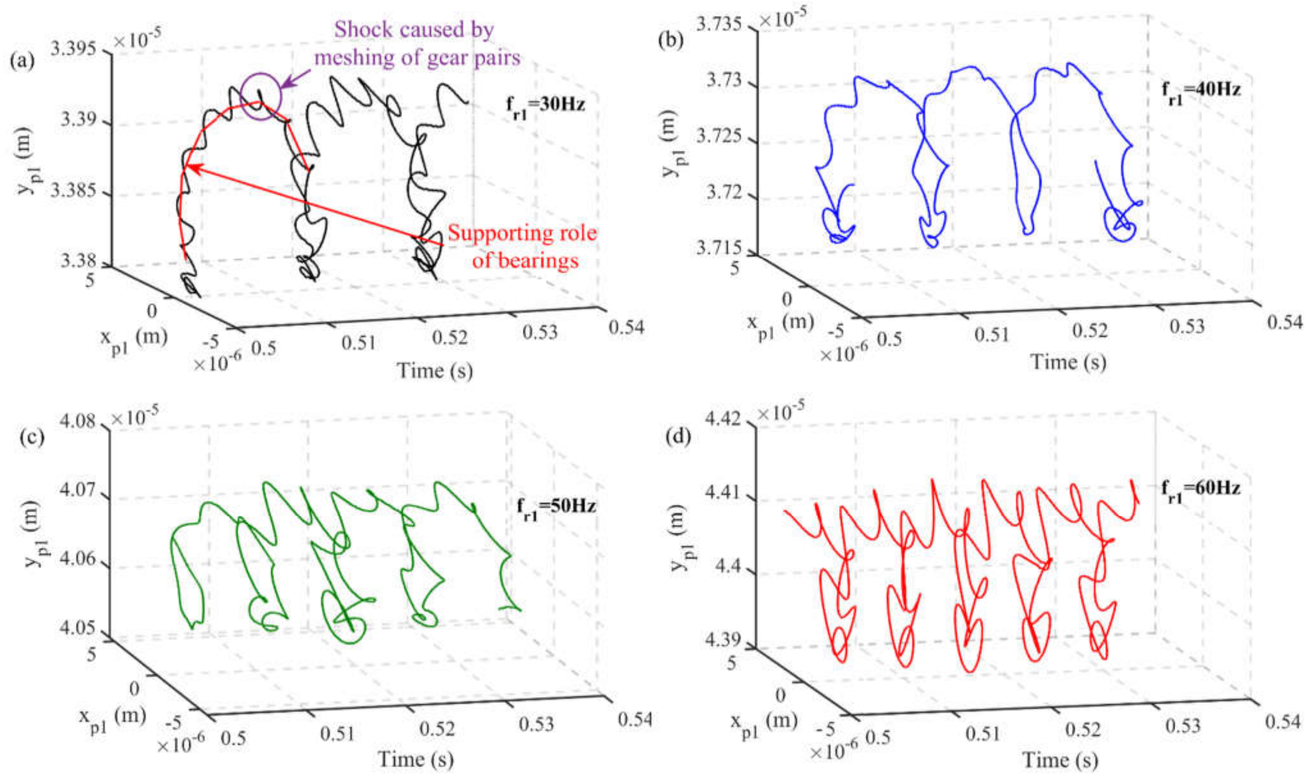

Figure 11. Axial track of outer ring: (a) f_{r1} = **30Hz**; (b) f_{r1} = **40Hz**; (c) f_{r1} = **50Hz**; (d) f_{r1} = **60Hz**.

5. Conclusion

In order to study the coupled vibration between the gear pair and the bearing in the gearbox, a 36 DOFs dynamic model of the gearbox is established in this paper. In this model, the nonlinear contact force of the bearing and the nonlinear meshing force of the gear pair are determined using the Hertz theory and the potential energy method, then the gyroscopic motion of the shaft caused by vibration of the bearing inner ring is used as the connection to establish the coupling relationship between the gear pair and the bearing. The generation mechanism of gear pair harmonic response and the vibration characteristics of the gearbox at different speeds are discussed in detail using this model. The main results are summarized as follows:

(1) In the gearbox, a closed control loop is formed due to the vibration transmission between the gear pair, the bearing and the shaft, there is a strong coupling relationship between the gear pair and the bearing. Each component emits excitation due to its own vibration and is also subject to interference from the closed loop.

(2) Due to the severe coupling relationship, the gyroscopic motion of the shaft is caused, which leads to the generation of center distance error and misalignment angle. Then the disorganized meshing process and the meshing stiffness excitation are affected, and the harmonic response of the gear pair is excited.

(3) When the speed of the gearbox is increased, the meshing process of the gear pair is more chaotic, and the stability of the gearbox is reduced. Although the vibration amplitude of the bearing and the gear pair is increased, the system mainly vibrates at the fundamental frequency, and the harmonics of the gear pair are also shifted to the low frequency band.

(4) The established model is confirmed by the Sawalhi model and experiments.

Author Contributions: Conceptualization, Y.S.; methodology, D. P.; software, Y.S.; validation, S.D.; formal analysis, Y.S. and D.P.; investigation, S.D. and W.J.; resources, W. J; data curation, S. J.; writing—original draft preparation, D.P.; writing—review and editing, Z.D. and S. J.; visualization, L.

H.; supervision, S.D. and L.H. project administration, Z.D. All authors have read and agreed to the published version of the manuscript.

Funding: The work described in this paper was supported by the Project of Guizhou Science and Technology Department (No. [2020]2Y041) and the Collaborative Innovation Fund project of Anhui Polytechnic University & Jiujiang District (No. 2022cyxtb3).

Institutional Review Board Statement: Not applicable.

Informed Consent Statement: Not applicable.

Conflicts of Interest: The authors declare no conflict of interest.

References

1. Chen, X.; Feng, Z. Induction motor stator current analysis for planetary gearbox fault diagnosis under time-varying speed conditions. MECH SYST SIGNAL PR. **2020**, 140: 106691.
2. Liang, X.; Zuo, M. J.; Feng, Z. Dynamic modeling of gearbox faults: A review. MECH SYST SIGNAL PR. **2018**, 98: 852-876.
3. Zheng, H.; Cheng, G.; Li, Y.; Liu, C. A fault diagnosis method for planetary gear under multi-operating conditions based on adaptive extended bag-of-words model. MEASUREMENT. **2020**, 156: 107593.
4. Liu, J.; Wang, L.; Ma, J.; Yu, W.; Shao, Y. A multi-body dynamic study of vibration of a planetary gear train with the planetary bearing fault. P I MECH ENG K-J MUL. **2019**, 233(3): 677-695.
5. Yi, Y.; Qin, D.; Liu C.Z. Investigation of electromechanical coupling vibration characteristics of an electric drive multistage gear system. MECH MACH THEORY. **2017**, 121: 446-459.
6. Wei, J.; Zhang, A.; Qin, D.; Lim, T. C.; Shu, R.; Lin, X.; Meng, F. A coupling dynamics analysis method for a multistage planetary gear system. MECH MACH THEORY. **2017**, 110: 27-49.
7. Jalan, A. K.; Mohanty, A. R. Model based fault diagnosis of a rotor-bearing system for misalignment and unbalance under steady-state condition. J SOUND VIB. **2009**, 327(3-5), 604-622.
8. Lu, W.; Zhang, Y.; Cheng, H.; Zhou, Y.; Lv, H. Research on dynamic behavior of multistage gears-bearings and box coupling system. MEASUREMENT. **2020**, 150: 107096.
9. Wang, C. Dynamic model of a helical gear pair considering tooth surface friction. J VIB CONTROL. **2020**, 26(15-16): 1356-1366.
10. Chen, Q.; Wang, Y.; Tian, W.; Wu, Y.; Chen, Y. An improved nonlinear dynamic model of gear pair with tooth surface microscopic features. NONLINEAR DYNAM. **2019**, 96(2): 1615-1634.
11. Ma, H.; Song, R.; Pang, X.; Wen, B. Time-varying mesh stiffness calculation of cracked spur gears. ENG FAIL ANAL. **2014**, 44: 179-194.
12. Ma, H.; Pang, X.; Zeng, J.; Wang, Q.; Wen, B. Effects of gear crack propagation paths on vibration responses of the perforated gear system. MECH SYST SIGNAL PR. **2015**, 62-63: 113-128.
13. Yu, W.; Mechefske, C. K.; Timusk, M. A new dynamic model of a cylindrical gear pair with localized spalling defects. NONLINEAR DYNAM. **2017**, 91(4): 2077–2095.
14. H., Endo; R., B., Randall; C., Gosselin. Differential diagnosis of spall vs. cracks in the gear tooth fillet region: Experimental validation. MECH SYST SIGNAL PR. **2009**, 23(3): 636-651.
15. PARKER, R. G.; VIJAYAKAR, S. M.; IMAJO, T. Nor-linear dynamic of response of a spur gear pair: modeling and experimental comparisons. J SOUND VIB. **2000**, 237(3): 435-455.
16. VAISHYA, M.; SINGH, R. SLIDING FRICTION-INDUCED NON-LINEARITY AND PARAMETRIC EFFECTS IN GEAR DYNAMICS. J SOUND VIB. 2001, 248(4): 671–694.
17. Xu, Zhang; Jiaxin, Zhong; Wei, Li; Mateusz, Bocian. Nonlinear dynamic analysis of high-speed gear pair with wear fault and tooth contact temperature for a wind turbine gearbox. MECH MACH THEORY. **2022**, 173.
18. Wen, C.; Meng, X.; Fang, C.; Gu, J., Xiao, L.; Jiang, S. Dynamic behaviors of angular contact ball bearing with a localized surface defect considering the influence of cage and oil lubrication. MECH MACH THEORY. 2021, 162, 104352.
19. Lu, Z.; Wang, X.; Yue, K.; Wei, J.; Yang, Z. Coupling model and vibration simulations of railway vehicles and running gear bearings with multitype defects. MECH MACH THEORY. **2021**, 157.
20. GUPTAP, K. Dynamic loads and cage wear in high-speed rolling bearings. WEAR. **1991**, 147: 119-134.
21. Niu, L.; Cao, H.; Hou, H.; Wu, B.; Lan, Y.; Xiong, X. Experimental observations and dynamic modeling of vibration characteristics of a cylindrical roller bearing with roller defects. MECH SYST SIGNAL PR. **2020**,138, 106553.
22. Wang, F.; Jing, M.; Yi, J.; Dong, G.; Liu, H.; Ji, B. Dynamic modelling for vibration analysis of a cylindrical roller bearing due to localized defects on raceways. P I MECH ENG K-J MUL. **2014**, 229(1), 39–64.
23. Shao, Y.; Liu, J.; Ye, J. A new method to model a localized surface defect in a cylindrical roller-bearing dynamic simulation. P I MECH ENG J-J ENG. **2013**, 228(2), 140–159.
24. Patel, V. N.; Tandon, N.; Pandey, R. K. A dynamic model for vibration studies of deep groove ball bearings considering single and multiple defects in races. J TRIBOL-T ASME. **2010**, 132(4): 041101.
25. Patil, M. S.; Mathew, J.; Rajendrakumar, P. K.; Desai, S. A theoretical model to predict the effect of the localized defect on vibrations associated with ball bearing. INT J MECH SCI. **2010**, 52(9): 1193-1201.

26. Tandon, N.; Choudhury, A. An analytical model for the prediction of the vibration response of rolling element bearings due to a localized defect. J SOUND VIB. **1997**, 205(3):275-292.
27. Patel, U. K. A.; Upadhyay, S. H. Upadhyay. Nonlinear dynamic response of cylindrical roller bearing-rotor system with 9 degree of freedom model having a combined localized defect at inner-outer races of bearing. TRIBOL T. **2017**, 60(2): 284-299.
28. Singh, S.; Kopke, U. G.; Howard, C. Q.; Petersen, D. Analyses of contact forces and vibration response for a defective rolling element bearing using an explicit dynamics finite element model. J SOUND VIB. **2014**, 333:5356-5377.
29. Singh, S.; Howard, C.Q.; Hansen, C.H.; Kopke, U.G. Analytical validation of an explicit finite element model of a rolling element bearing with a localised line spall. J SOUND VIB. **2018**, 416: 94-110.
30. Xiang, L.; Gao, N. Coupled torsion–bending dynamic analysis of gear-rotor-bearing system with eccentricity fluctuation. APPL MATH MODEL. **2017**, 50: 569–584.
31. Baguet, S.; Jacquenot, G. Nonlinear couplings in a gear-shaft-bearing system. MECH MACH THEORY. **2010**, 45(12): 1777-1796.
32. Cui, L.; Zhang, Y.; Zhang, F.; Zhang, J.; Lee, S. Vibration response mechanism of faulty outer race rolling element bearings for quantitative analysis. J SOUND VIB. **2016**, 364: 67–76.
33. Wang, F.; Jing, M.; Fan, H.; Wei, Y.; Zhao, Y., Liu, H. Investigation on contact angle of ball bearings. P I MECH ENG K-J MUL. **2017**, 231(1): 230-251.
34. Dai, P.; Wang, J.; Yan, S.; Huang, S., Wang, F., Liu, J. Vibration characteristics of the gear shaft-bearing system with compound defects under variable operating conditions. P I MECH ENG K-J MUL. **2022**, 236(1):113-129.
35. Wen, Q.; Du, Q.; Zhai, X. Analytical calculation of the tooth surface contact stress of spur gear pairs with misalignment errors in multiple degrees of freedom. MECH MACH THEORY. **2020**, 149, 103823.
36. Saxena, A.; Parey, A.; Chouksey, M. Effect of shaft misalignment and friction force on time varying mesh stiffness of spur gear pair. ENG FAIL ANAL. **2015**, 49, 79–91.
37. Dai, P.; Wang, J.; Yan, S. Effects of Localized Defects of Gear-Shaft-Bearing Coupling System on the Meshing Stiffness of Gear Pairs. J. Vib. Eng. Technol. **2022**, 10: 1153–1173.
38. Wang, C. Dynamic model of a helical gear pair considering tooth surface friction. J VIB CONTROL. **2020**, 26(15-16): 1356-1366.
39. Chen, Q.; Wang, Y.; Tian, W.; Wu, Y.; Chen, Y. An improved nonlinear dynamic model of gear pair with tooth surface microscopic features. NONLINEAR DYNAM. **2019**, 96(2): 1615-1634.
40. Wang, L.; Shao, Y. Fault mode analysis and detection for gear tooth crack during its propagating process based on dynamic simulation method. ENG FAIL ANAL. **2017**, 71:166–178.
41. A., Z., Hajjaj; K., Corrigan; M., Mohammadpour; S., Theodossiades. On the stability analysis of gear pairs with tooth profile modification. MECH MACH THEORY. **2022**, 174,104888.
42. Sawalhi, N.; Randall, R. B. Simulating gear and bearing interactions in the presence of faults. MECH SYST SIGNAL PR. **2008**, 22(8): 1952-1966.